

The ISO–SWS spectrum of planetary nebula NGC 7027*

J. Bernard Salas^{1,2}, S. R. Pottasch², D. A. Beintema¹, and P. R. Wesselius¹

¹ SRON Laboratory for Space Research, PO Box 800, 9700 AV Groningen, The Netherlands

² Kapteyn Astronomical Institute, PO Box 800, 9700 AV Groningen, The Netherlands

Received 19 July 2000 / Accepted 27 November 2000

Abstract. We present the infrared spectrum of the planetary nebula NGC 7027 observed with the Short Wavelength Spectrometer (SWS), on board the Infrared Space Observatory (ISO). These data allow us to derive the electron density and, together with the IUE and optical spectra, the electron temperature for several ions. The nebular composition has been determined, the evolutionary status of the central star is discussed and the element depletion in the nebula is given. We conclude that the progenitor was a C-rich star with a mass between 3 and 4 M_{\odot} .

Key words. ISM: abundances – planetary nebulae: individual: NGC 7027 – infrared: ISM: lines and bands

1. Introduction

NGC 7027 is a well known planetary nebula. It is very young, dense and has an extremely rich and highly ionized spectrum due to its hot central star. The nebula has some features that makes it very interesting. The rich spectrum has been used several times to give insight about the evolution and original status of its central star. For this purpose accurate abundances are needed, and the distance, in order to know the intrinsic luminosity, has to be accurately measured. Abundance studies have been made before, but using the near-infrared SWS-ISO data the temperature uncertainty can be avoided as well as other problems, therefore achieving an accurate measurement of the nebular abundances. These ISO advantages are presented by Pottasch & Beintema (1999) and we summarize them here:

1. Extinction effects are absent from most of the spectrum in contrast to the visible and UV spectra;
2. Many stages of ionization are observed, reducing strongly the need for uncertain corrections for unseen stages of ionization;
3. Electron temperature fluctuations, or uncertainties, are much less as important than in the optical or ultraviolet spectra. The infrared lines originate from levels so close to the ground level, that to populate these

levels, the electron temperature does not play an important role;

4. Only in a few cases (Ar v and Ne v) is there an important density dependence.

In the second and third sections of this paper the observations and main reduction techniques are described. Data on the infrared lines are listed in section four while the visual and ultraviolet lines used are given in section five. In the sixth section the electron temperature and density as well as the ionic and element abundances are derived. These results are discussed in section seven and the abundances are compared with an evolutionary model in an attempt to derive the mass of the progenitor star of NGC 7027.

2. ISO observations

The data were obtained in the ISO guaranteed time in spring 1997. The observations were made with the Short Wavelength Spectrometer (de Graauw et al. 1996) covering the range 2.38 to 45.2 μm , using the SWS01 observing template, which provides a spectral resolution from 1000 to 2500. From all NGC 7027's observations, the one used in this paper (TDT number 55800537) was chosen because of its highest signal to noise ratio.

NGC 7027's infrared size is sufficiently smaller than the different sizes of the apertures used with SWS to offer no problem. A VLA radio image of NGC 7027 at 14.7 GHz obtained by Roelfsema et al. (1991) clearly stays within the ISO–SWS small aperture $14'' \times 20''$. The other SWS apertures are larger, $14'' \times 27''$, $20'' \times 27''$ and $20'' \times 33''$. They are all centered at almost the same position within

Send offprint requests to: J. Bernard Salas,
e-mail: J.Bernard@srn.rug.nl

* Based on observations with ISO, an ESA project with instruments funded by ESA Member States (especially the PI countries: France, Germany, The Netherlands and the UK) and with the participation of ISAS and NASA.

Table 1. Comparison of present SWS observations with those of Persi et al. (1999) taken with ISOCAM–CVF. Flux units are in 10^{-12} erg cm $^{-2}$ s $^{-1}$

Line (μm)	Ident.	Present observ.	Persi et al. (1999)
4.05	Br α	91.6	66
5.61	[Mg v]	416	318
6.98	[Ar II]	30.7	180
7.65	[Ne VI]	96.5	2161
8.99	[Ar III]	122	80
10.51	[S IV]	429	637
12.81	[Ne II]	91.6	177
14.32	[Ne v]	1350	1499
15.56	[Ne III]	1090	1132

an uncertainty of $3''$. Persi et al. (1999) studied the infrared size of NGC 7027 using spectral images taken with the ISOCAM–CVF, showing that it has an ellipsoidal morphology of about $9'' \times 11''$. This is again within the smallest ISO–SWS aperture. Persi et al. (1999) measured the spectra over an area of 25 square arcsec that with no doubt contains the whole nebula. A comparison of present fluxes with those found by Persi et al. (1999) is shown in Table 1 and demonstrate that no flux is missing in the SWS observation.

In present observations the Br α (measured with the smallest SWS aperture), [Mg v] and [Ar III] are stronger than those of Persi et al. (1999), indicating that no flux is being lost in the present observations. Strong differences in both measurement are probably due to the poor spectral resolution of the ISOCAM–CVF in comparison with the SWS, and therefore the latter are more accurate. The extremely high flux of [Ne VI] measured by Persi et al. (1999) is wrong because it is blended with a PAH feature. No contributions from the outer parts of the nebula are expected since the gas is cold and therefore the whole flux is seen in each aperture. For all these reasons no aperture correction for the infrared lines is needed.

The IUE observations were taken at almost the same position as our observations. The aperture of the IUE is an ellipse of $10'' \times 23''$ very similar to our smallest aperture. It therefore contains the whole nebula. The optical lines were observed with a very small aperture on the bright part of NGC 7027 and represent a part of the nebula. We assume that they are representative of the entire nebula. Using the entire H β flux, they are scaled to the total flux. We avoid here making any aperture corrections because these are expected to be small if they exist at all.

3. Data reduction

The data were reduced using the available tools in the inter-active analysis software package distributed by the SWS consortium. Our reduction differs from the stan-

dard pipeline in the removing of fringing in the data, and a better flatfielding. Any step in the reduction analysis which could affect the spectral resolution or the linearity of the data was avoided. Line fluxes were measured fitting Gaussians to the observed line profiles using the routine *multi_fit*. It allows removal of glitches or bad data interactively in each line. This was rather time consuming, but the weakest lines were found and the highest possible resolution kept at each wavelength.

The reduction didn't present any problem except in the first part of band $2c$ (7 to 12 μm) where the up and down scans deviated significantly from each other, but matched in the rest of the band when flatfielding was applied. This doesn't affect the measured fluxes but could be important when reasonable upper limits to some lines are determined, as explained in next paragraph. This was caused by some detectors (19, 20, 21, 23 and 24) which suffered from erroneous dark current subtraction. The range 7.3 to 7.6 μm was affected. These detectors were removed. A reference flat (order one) was defined using the remaining detectors and applied to the whole band. Flatfielding reduces the mismatch and then all detectors could be used to measured line intensities.

It is useful to compute an upper limit to the flux for some unseen lines. For this purpose, outlying data points were removed with the *sigclip* tool and the spectra were rebinned (*sws_rebin* tool) to a standard resolution. Upper limits for the lines [Cl IV] 11.76 μm , [Na VI] 8.61 μm , [K VI] 5.58 and 8.83 μm were calculated using a model of a synthetic Gaussian, with the width corresponding to the resolution, and a height of three times the rms (deviation from the average). These upper limits of unseen lines allow to more accurately apply the ionization correction factor for the relevant ions.

4. Line flux discussion

In Table 2 the fluxes measured for the infrared (IR) lines are listed. In total around 80 lines were measured. Calibration errors are larger at longer wavelengths but on average amount to about 20%. Random measurement errors depend on the flux strength: weak lines ($I < 5$, where I is in 10^{-12} erg cm $^{-2}$ s $^{-1}$) have estimated errors of about 20%, intermediate lines ($5 < I < 10$) of about 10%, while the strongest lines ($I > 10$), have normally less than 5% uncertainty. All the lines follow this behavior with the exception of the S III line at 33.5 μm with a measured intensity of $7.12 \cdot 10^{-12}$ erg cm $^{-2}$ s $^{-1}$ and an uncertainty of 19%. This part of the spectrum is the noisiest and weak lines are not seen. Therefore, this line could be considered an intermediate strength line in this part of the spectrum. Thus the uncertainty in the fluxes of intermediate and strong lines is dominated by the calibration error.

NGC 7027's spectrum is extremely rich as can be seen in Fig. 1. The hydrogen and helium lines are abundant in the whole spectrum but specially in the range 2.4–5.5 μm . Ions with high stages of ionization are found (i.e. Fe VII, Na VII, Ar VI) in the nebula. Nine molecular hydrogen lines

Table 2. Line fluxes for NGC 7027

λ (μm)	Ident.	Flux (10^{-12} erg cm^{-2} s^{-1})	λ (μm)	Ident.	Flux (10^{-12} erg cm^{-2} s^{-1})
2.406	H ₂ , 1→0 Q(1)	3.73	5.580	[K VI]	< 8.28
2.424	H ₂ , 1→0 Q(3)	2.35	5.908	H I 6–9	6.53
2.495	H I 5–17	1.17	5.981	[K IV]	3.60
2.564	H I 5–15	2.52	6.705	[Cl V]	6.09
2.613	He I 4–6	1.46	6.910	H ₂ , 0→0 S(5)	6.69
2.626	H I (Br β)	45.9	6.947	He II 8–9	3.47
2.671	He I 4–6	1.45	6.985	[Ar II]	30.7
2.675	H I 5–13	2.24	7.317	[Na III]	13.9
2.758	H I 5–12	2.84	7.459	H I (Pf α)	28.3
2.802	H ₂ , 1→0 O(3)	2.96	7.503	H I 6–8	8.91
2.826	He II 7–9	5.43	7.652	[Ne VI]	96.5
2.905	[Al V]	1.16	7.814	[Fe VII]	2.63
3.004	H ₂ , 1→0 O(4)	0.59	7.901	[Ar V]	47.1
3.039	H I 5–10	5.70	8.025	H ₂ , 0→0 S(4)	2.52
3.092	He II 6–7	18.8	8.610	[Na VI]	< 3.45
3.095	He II 8–11	1.66	8.761	H I 7–10	2.53
3.207	[Ca IV]	1.47	8.830	[K VI]	< 4.17
3.234	H ₂ , 1→0 O(5)	0.79	8.991	[Ar III]	122
3.625	H I 6–20, 6–19	0.95	9.042	[Na IV]	12.1
3.740	H I (Pf γ)	11.0	9.525	[Fe VII]	4.85
3.749	H I 6–17	0.78	9.665	H ₂ , 0→0 S(3)	6.82
3.907	H I 6–15	1.29	9.713	He II 9–10	2.16
4.020	He I 4–5	1.08	10.510	[S IV]	429
4.022	H I 6–14	0.72	11.760	[Cl IV]	< 4.16
4.038	He I 4–5	0.97	12.372	H I 6–7	11.3
4.052	H I (Br α)	91.6	12.812	[Ne II]	91.6
4.296	He I 3–5	4.86	13.101	[Ar V]	31.0
4.377	H I 6–12	1.66	13.520	[Mg V]	38.7
4.486	[Mg IV]	148	14.321	[Ne V]	1350
4.529	[Ar VI]	126	15.550	[Ne III]	1090
4.618	[K III]	4.09	18.713	[S III]	76.0
4.654	H I (Pf β)	17.5	19.062	H I 7–8	5.94
4.672	H I 6–11	2.50	21.800	[Ar III]	3.00
4.764	He II 7–8	9.43	24.315	[Ne V]	387
5.128	H I 6–10	4.51	25.888	[O IV]	715
5.510	H ₂ , 0→0 S(7)	2.29	33.477	[S III]	7.12
5.610	[Mg V]	416	34.812	[Si II]	14.9
			36.012	[Ne III]	49.2

(H₂) have been measured as well and probably originate in the outer part of the nebula where the temperature is lowest. For Ar, K and specially Ne we have information for the most important stages of ionization implying that the uncertainty in the ionization correction factor (ICF) used to derive the absolute abundances will be much reduced. Several stages of ionization of some ions were not observe. Then, an upper limit to the flux was determined, as described in the previous section. Also noticeable in the spectrum is the strong continuum at the longest wavelength and the features at 3.3, 6.6, 7.7, 8.8 and 11.2 μm now known as PAHs as well as a broad PAH plateau from 15 to 20 μm . In this paper we will concern ourselves only with the emission lines. A detail study of the PAHs and the plateau can be found in the articles by Peeters et al. (2001), Hony et al. (2001) and Van Kerckhoven et al. (2000).

5. The visual and the ultraviolet spectrum

In addition to the large number of infrared lines measured, also some optical and ultraviolet lines were used taken from the paper of Keyes & Aller (1990). The information on such important ions as C, N, O is mainly derived from optical and ultraviolet data.

The lines used are listed in Table 3. To correct optical fluxes for interstellar extinction a value of $C = 1.25$ (where $C = \log(\frac{F(\text{H}\beta)_{\text{predicted}}}{F(\text{H}\beta)_{\text{observed}}})$) was used, which leads to an extinction of $E_{B-V} = 0.85$. To calculate this the H β flux was computed in two ways. Using the equation given by Pottasch (1984):

$$F(\text{H}\beta) = \frac{S_\nu}{2.82 \cdot 10^9 \cdot t^{0.53} \left(1 + \frac{\text{He}^+}{\text{H}^+} + 3.7 \frac{\text{He}^{++}}{\text{H}^+}\right)} \quad (1)$$

where $S_\nu = 5.7$ Jy at 5 GHz (Baars et al. 1977), t is the temperature of the nebula in 10^4 K and $2.82 \cdot 10^9$ is

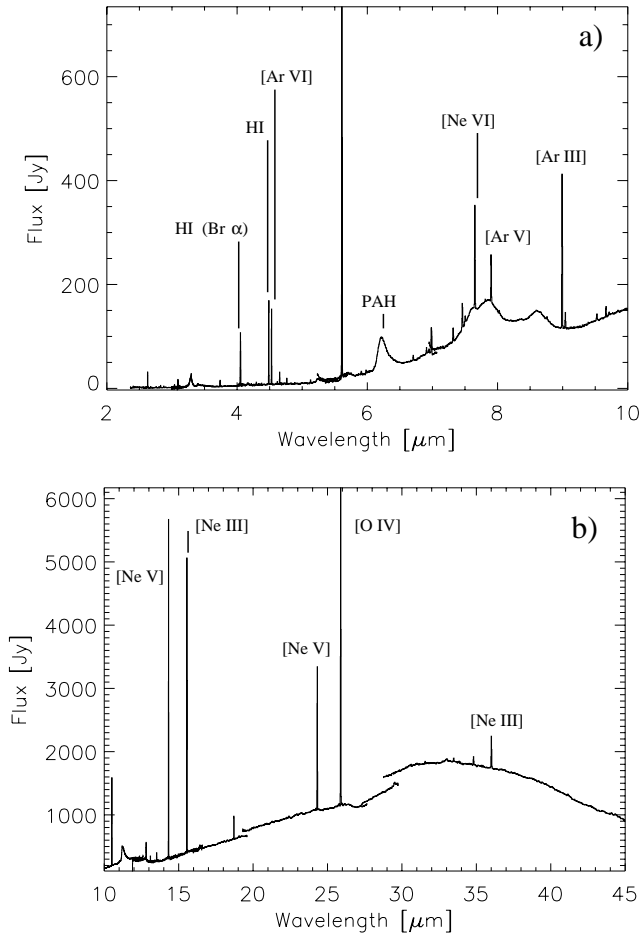


Fig. 1. SWS spectrum of NGC 7027. As can be seen strong lines of high ionization stages of some ions are seen. Hydrogen lines are abundant. Also noticeable the strong continuum at longer wavelength and PAHs at 6.6, 7.7 and 8.8 μm

a conversion factor which allows to write the flux density S_ν in Jy and the $F(\text{H}\beta)$ in $\text{erg cm}^{-2} \text{s}^{-1}$. Applying Eq. (1) leads to $F(\text{H}\beta) = 1.34 \cdot 10^{-9} \text{ erg cm}^{-2} \text{s}^{-1}$. The helium abundances are taken from Table 6. Also, the $\text{H}\beta$ flux can be determined by comparing the infrared hydrogen lines of different series (presented in Table 2), with theoretical predictions given by Hummer & Storey (1987) for a black body case B at a temperature of 15 000 K and an electron density of $10\,000 \text{ cm}^{-3}$. The results are shown in Table 4.

The average of these measurements leads to $\overline{F(\text{H}\beta)} = 1.27 \cdot 10^{-9} \text{ erg cm}^{-2} \text{s}^{-1}$. The $\text{Br}\alpha$ line observed (using no reddening correction) is the strongest and therefore has been most accurately measured. The value of $F(\text{H}\beta) = 1.35 \cdot 10^{-9} \text{ erg cm}^{-2} \text{s}^{-1}$ deduced from this line agrees with the one derive from Eq. (1) and was finally adopted. It is worth mention here that the theoretical predictions from Hummer & Storey (1987) are given just for $N_e = 10^4$ or 10^5 cm^{-3} . Here a N_e of 10^4 cm^{-3} is used but an $N_e = 10^5 \text{ cm}^{-3}$ would lead to the same conclusions ($\overline{F(\text{H}\beta)} = 1.27 \cdot 10^{-9} \text{ erg cm}^{-2} \text{s}^{-1}$). The optical lines were corrected for reddening using the extinction law of Fluks et al. (1994) and an extinction of $E_{B-V} = 0.85$. A recent publication of Wolff et al. (2000) derives an extinction of

Table 3. Ultraviolet (IUE) and optical line fluxes (Keyes & Aller 1990). Keyes fluxes were dereddened fluxes using an interstellar extinction of $E_{B-V} = 0.85$

Wavelength (nm)	Ident.	Measured Fluxes ¹	Dereddened Intensities ¹
123.83	N v	0.12	600
140.06	O iv	< 0.61	< 990
148.50	N iv	0.71	880
154.83	C iv	13.4	22 000
157.57	[Ne v]	0.21	100
164.20	He ii	5.00	4600
174.95	N iii	0.62	540
189.20	Si iii	0.17	200
190.88	C iii	6.88	14 000
232.55	C ii	0.62	1200
242.45	[Ne iv]	–	28
334.68	[Ne v]	–	700
342.68	[Ne v]	–	2100
372.70	[O ii]	7.88	220
386.98	[Ne iii]	57.1	1500
396.86	[Ne iii]	20.5	500
436.44	[O iii]	17.6	340
447.10	He i	2.50	45.4
468.60	He ii	42.6	660
471.14	[Ar iv]	33.9	38.1
474.00	[Ar iv]	119.9	131.7
486.10	$\text{H}\beta$	75.9	1360
493.26	[O iii]	512	2.9
496.03	[O iii]	0.23	6400
500.82	[O iii]	1553	19 000
553.80	[Cl iii]	1.01	8.6
658.40	[N ii]	267	1500
673.10	[S ii]	10.8	56
857.70	[Cl ii]	1.33	3.6

⁽¹⁾ Units: $10^{-12} \text{ erg cm}^{-2} \text{s}^{-1}$.

Table 4. Derivation of $\text{H}\beta$ fluxes. Predicted $\text{Br}\alpha$, $\text{Br}\beta$, $\text{Pf}\alpha$, $\text{Pf}\beta$, $\text{Pf}\gamma$ fluxes from Hummer & Storey (1987) for a black body at $T_e = 15\,000 \text{ K}$ and $N_e = 10\,000 \text{ cm}^{-3}$

Ident.	Transition	λ (μm)	Predic. flux w.r.t. $\text{H}\beta$	Flux ¹	$F(\text{H}\beta)^2$
$\text{Br}\alpha$	$5 \rightarrow 4$	4.052	$6.77 \cdot 10^{-2}$	91.6	1.35
$\text{Br}\beta$	$6 \rightarrow 4$	2.626	$4.00 \cdot 10^{-2}$	45.9	1.15
$\text{Pf}\alpha$	$6 \rightarrow 5$	7.459	$2.09 \cdot 10^{-2}$	28.3	1.35
$\text{Pf}\beta$	$7 \rightarrow 5$	4.654	$1.37 \cdot 10^{-2}$	17.5	1.28
$\text{Pf}\gamma$	$8 \rightarrow 5$	3.740	$9.20 \cdot 10^{-3}$	11.0	1.20

¹ Units in $10^{-12} \text{ erg cm}^{-2} \text{s}^{-1}$.

² Units in $10^{-9} \text{ erg cm}^{-2} \text{s}^{-1}$.

$E_{B-V} = 1.10$ for NGC 7027 by directly measuring the central star. This difference is difficult to explain and would considerably change the values of the dereddened fluxes. One possibility is that NGC 7027 shows variations in the extinction across the nebula (Wolff et al. 2000). This can be higher towards the central star region than in the nebula itself. Wolff et al. (2000) give a summary of extinction

Table 5. Electron density. $T_e = 15\,500$ K is used

Ion	Ion Pot (eV)	Lines used (nm)	Observed ratio	N_e (cm^{-3})
S II	10.4	673.1/671.6	2.27	40 000 ¹
O II	13.6	372.6/372.9	2.74	25 000 ²
Cl III	23.8	553.8/551.8	3.90	80 000 ¹
C III	24.4	190.7/190.9	0.62	75 000
Ne III	41.0	15 500/36 000	22.2	75 800
K VI	82.7	560.4/622.8	–	40 000 ¹
Ne V	97.1	24 300/14 300	0.29	26 900

¹ Values taken from Keyes & Aller (1990).

² Value taken from Keenan et al. (1999).

determinations by several authors: Walton et al. (1988) find an extinction $E_{B-V} = 0.8$ for the central star and $\langle E_{B-V} \rangle = 1.02$ for the rest of the nebula, Kaler & Lutz (1985) found 0.85 and Shaw & Kaler (1982) 0.94.

According to Keyes et al. (1990) the UV lines have errors less than 20%, while the optical lines have errors below 50%. Here a 15% error is assumed for the UV, and a 40% error for the optical lines. Also the N III infrared line at $57.3 \mu\text{m}$ from the Long Wavelength Spectrometer (LWS, 43 to $196.7 \mu\text{m}$) has been used. It was taken from Liu et al. (1996) and was used to compare the abundance with that found using the ultraviolet line at 1750 \AA .

6. Analysis

Using the entire data set (infrared, optical and ultraviolet) the physical parameters (electron density and temperature) have been determined as a function of the ionization potential.

6.1. Electron density

An electron temperature of $15\,500$ K has been chosen to compute the density. This choice is justified in the next subsection. To determine the electron density (N_e) reliably, the ratio of lines close in energy level is needed so that the temperature hardly plays a role in populating these levels. Two ions, Ne III and Ne V fulfil this condition. In addition the N_e for C III was calculated using ultraviolet lines (Keyes & Aller 1990). These measurements cover the ionization potential (IP) range from 23 to 97 eV. In order to have information on the N_e for ions with low IP the values given by Keenan et al. (1999) for O II, and Keyes et al. (1990) for S II, Cl III were used. All derived N_e values are shown in Table 5.

Table 5 does not show a trend of N_e with IP in the range 10 to 23 eV, but from 23 to 97 eV a trend appears when the value of K VI of Keyes et al. (1990) is used. In this range N_e seems to drop from a value of 75 000 to $25\,000 \text{ cm}^{-3}$. To compute abundances for each ion a N_e is needed. Because many infrared lines are used, the N_e is not

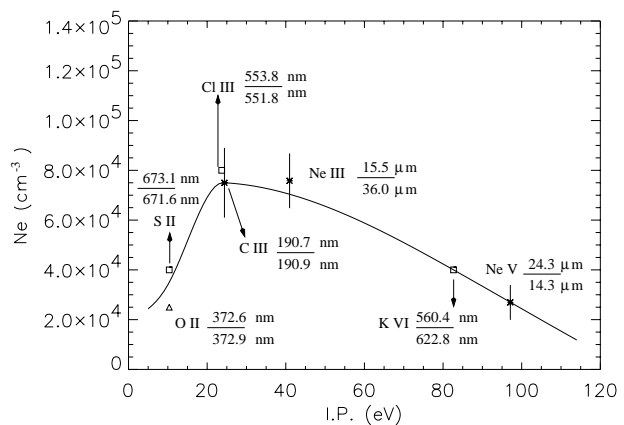


Fig. 2. Electron density versus ionization potential. The ratios used for each ion are indicated. Asterisks are our measurements while the triangle show N_e value derived by Keenan and the squares gives the values by Keyes. The shape of the assumed curve is in accordance with the expected physical behaviour (see discussion Sect. 7.2)

critical, and the relative abundance of the ions do usually not strongly depends on it. N_e was derived from the curve in Fig. 2. Most of the ions are not N_e dependent (only three ions show N_e dependence, Ar V, O IV and Ne V). For this reason an average $N_e = 50\,000 \text{ cm}^{-3}$ was used to compute the electron temperature (following subsection).

6.2. Electron temperature

To compute the electron temperature (T_e) line ratios are needed originating from energy levels differing by several electron volts. Using optical data only two ions (N II and O III) obey this condition while using infrared and ultraviolet data, three others (O IV, Ne V and Mg V) become available as well. As can be seen from Fig. 3 these provide information on almost the whole IP range of interest. In Fig. 3 we present T_e as a function of IP. The density used is $50\,000 \text{ cm}^{-3}$ (see previous section). There exists a correlation between T_e and IP, such that T_e increases until about 70 eV and then remains at a constant value of $15\,500$ K.

Some ions need a further discussion. O IV gives a higher temperature and this may be because the ultraviolet line at 140.0 nm is blended with Si IV. Only Ne V rather strongly depends on N_e . For this ion the average density, $N_e = 50\,000 \text{ cm}^{-3}$ is used. Using $N_e = 30\,000 \text{ cm}^{-3}$ leads to a much higher T_e of $22\,400$ K. The Ne III ratio, 386.8 nm over $15.5 \mu\text{m}$ can, in principle, be used to derived T_e . As noticed before by Pottasch & Beintema (1999), it always gives a low temperature. In this study $T_e = 11\,500$ has been found using this ratio. This has been found in many nebulae, i.e. NGC 6302, NGC 6537. It is not clear why, but it may have something to do with the uncertainty in the atomic parameters and the 386.8 nm line has not been used in this paper.

Table 6. Ionic and element abundances

Ion	λ (nm)	$N_{\text{ion}}/N_{\text{p}}$	$\sum N_{\text{ion}}/N_{\text{p}}$	ICF ¹	$N_{\text{elem.}}/N_{\text{p}}$
He ⁺	447.2	0.0639 ^a			
He ⁺⁺	468.6	0.0422 ^a	0.106	1	0.106
Ca ³⁺	3200	1.1(-8)	–	–	–
Mg ³⁺	4490	4.7(-6)			
Mg ⁴⁺	5610	6.3(-6)	1.1(-5)	2	2.2(-5)
Ar ⁺	6980	1.7(-7)			
Ar ⁺⁺	8990	1.1(-6)			
Ar ³⁺	471.1, 474.0	7.4(-7)			
Ar ⁴⁺	7900	1.6(-7)			
Ar ⁵⁺	4530	1.3(-7)	2.3(-6)	1	2.3(-6)
K ⁺⁺	4620	2.2(-8)			
K ³⁺	5980	1.4(-8)			
K ⁵⁺	5580, 8830	< 1.2(-8)	3.6(-8)	1.35	4.9(-8)
Na ⁺⁺	7320	6.9(-7)			
Na ³⁺	9040	3.3(-7)			
Na ⁵⁺	8610	< 3.4(-8)	1.0(-6)	1.2	1.2(-6)
Ne ⁺	12 800	9.6(-6)			
Ne ⁺⁺	15 500, 36 000	6.9(-5)			
Ne ³⁺	242.5	2.7(-6)			
Ne ⁴⁺	24 300, 14 300	1.5(-5)			
Ne ⁵⁺	7650	8.7(-7)	1.0(-4)	1	1.0(-4)
Fe ⁶⁺	7810, 9520	2.8(-7)	–	–	–
S ⁺	673.1	6.8(-7)			
S ⁺⁺	18 700, 33 400	3.6(-6)			
S ³⁺	10 500	3.1(-6)	7.4(-6)	1.27	9.4(-6)
O ⁺	372.7	3.4(-5)			
O ⁺⁺	500.8, 493.2	1.8(-4)			
O ³⁺	25 900	1.3(-4)			
O ³⁺	140.0	< 4.2(-4)	3.5(-4)	1.17	4.1(-4)
Si ⁺	34 800	3.0(-6)			
Si ⁺⁺	189.2	2.1(-6)	5.2(-6)	1.2	6.2(-6)
N ⁺	658.4	2.0(-5)			
N ⁺⁺	57 300	9.1(-5)			
N ³⁺	148.7	3.5(-5)			
N ⁴⁺	123.8	1.6(-5)	1.6(-4)	1	1.6(-4)
C ⁺	232.5	1.1(-4)			
C ⁺	157 700	5.9(-3)			
C ⁺⁺	190.9	3.4(-4)			
C ³⁺	154.8	0.7(-5)	5.2(-4)	1.15	6.0(-4)
Cl ⁺	857.7	8.4(-9)			
Cl ⁺⁺	554.0	6.4(-8)			
Cl ³⁺	11 800	< 4.4(-8)			
Cl ⁴⁺	6700	1.7(-8)	8.9(-8)	1.23	1.1(-7)

¹ ICF = Ionization Correction Factor.^a Using the predictions for the helium emission lines given by Benjamin et al. (1999).

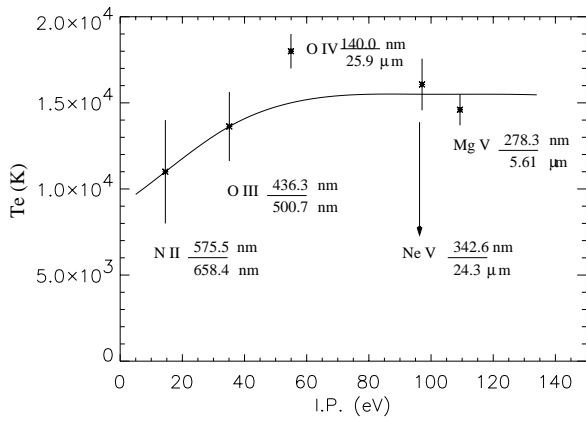


Fig. 3. Electron temperature versus ionization potential. The lines used for each ion are indicated. There is a correlation of T_e with IP, represented by the curve

6.3. Abundances

In order to be able to compute abundances, values of N_e and T_e are needed for each ion. They are derived from the relations presented in Figs. 2 and 3. Once the N_e and T_e are known the relative ionic abundances can be determined. Then, applying an ICF the element abundances are derived. Ionic abundances are normalized to hydrogen. The equation used to determine the ionic abundances is:

$$\frac{N_{\text{ion}}}{N_p} = \frac{I_{\text{ion}}}{I_{H\beta}} N_e \frac{\lambda_{ul}}{\lambda_{H\beta}} \frac{\alpha_{H\beta}}{A_{ul}} \left(\frac{N_u}{N_{\text{ion}}} \right)^{-1}. \quad (2)$$

In the equation N_p is the density of the ionized hydrogen; $I_{\text{ion}}/I_{H\beta}$ is the measured intensity of the ionic line, normalized to $H\beta$; λ_{ul} is the wavelength of the line and $\lambda_{H\beta}$ is the wavelength of $H\beta$; $\alpha_{H\beta}$ is the effective recombination coefficient for $H\beta$; A_{ul} is the Einstein spontaneous transition rate for the line and finally N_u/N_{ion} is the ratio of the population of the level from which the line originates to the total population of the ion.

All abundance values are shown in Table 6. The ICF is unity in four cases, because all important ionization states have been measured. In most cases it is between 1.0 and 1.25, and only in three cases is it above 1.25 (S, Mg and K with ICF's of 1.27, 2 and 1.35 respectively). In Keyes & Aller (1990), the ICF is normally between 1.2 and 5, and only in a few cases is under 1.2. This shows that the present abundance determination is an important improvement. The ICF were calculated on a purely empirical basis. For a given element the ionization potential where the maximum ionic abundance is reached was taken into account. For some ions like potassium, no information on the high sixth stage of ionization was found, thus an upper limit on K^{5+} was derived. As can be seen from Table 6, the contribution of the K^{5+} ion should not exceed 1.2(–8). The contribution of this to the element abundance was constrained. For Calcium and Iron the abundance has not been determined because important contributions from other stages of ionization are expected.

Si^+ gives almost the same ionic abundance as the Si^{2+} ion. This is suspicious because of the low electron temperature needed to excite this ion, and it probably originates mainly from the photodissociation region outside the nebula since the Si^+ ion is ionized at a low potential (8.1 eV).

Comparison with the nitrogen ions that have similar ionization potentials shows that N^{2+} gives a major contribution, while that of N^+ is not negligible but lower than other ions. Silicon should follow the same behavior, and the Si^+ contribution is probably coming from the photodissociation region around NGC 7027 instead of from the nebula itself. These considerations lead to lower abundances of C and Si (see Table 7).

A comparison of these abundances with those found in the Sun, O–B stars, and those of Keyes & Aller (1990) and Middlemass (1990) is shown in Table 7. The helium abundance agrees with the earlier results of Keyes & Aller (1990) and Middlemass (1990). Carbon is abundant, with a value similar to that found by Keyes & Aller (1990) but lower than found by Middlemass (1990). The model of Middlemass predicts a high abundance of all carbon ions, including C II. The abundance of oxygen is lower than in the Sun. This has also been found for many PNe in the past (Aller & Hyung 1995) and is in reasonable agreement with Keyes & Aller and Middlemass. The nitrogen, neon, magnesium, silicon and argon abundances are in agreement with the other authors. The magnesium abundance is lower than the one found in the Sun but similar to that of the O, B stars, supporting the idea that this element is depleted onto dust. The same is true for silicon, its abundance is even lower than found in O, B stars. This element is a well known component of the dust and the missing silicon is probably in this form.

In Table 8 abundance ratios are compared with the Sun and O, B stars. The ratio of N/O is almost twice as high as that found in the Sun and O, B stars, while the C/O ratio is three times high. This means that nitrogen and carbon are over-abundant in the nebula and it is likely that some oxygen has been converted into nitrogen in the course of its evolution by the CNO cycle. This is supported by the fact that the (C+N+O)/H ratio is very similar to solar indicating a similar mass of the progenitor star of the nebula. The solar O is over abundant and could explain the difference in ratios.

7. Discussion

The derived parameters, electron density and temperature, are shown in Table 5, Figs. 2 and 3 respectively. The ionic and element abundances of NGC 7027 are given in Table 6.

7.1. Missing stages of ionization

Ionization correction factors were needed in the past to obtain the abundance of an element, when only one or a few stages of ionization were observed. These were used to estimate the contribution of these unobserved stages of

Table 7. Comparison of abundances in NGC 7027

Element	Present abund.	Sun ¹	O, B Stars ²	Keyes & Aller (1990)	Middlemass (1990)
Helium	0.106	0.098		0.111	0.104
Carbon	6.0(-4)	3.55(-4)	1.74(-4)	6.9(-4)	1.3(-3)
Nitrogen	1.6(-4)	9.33(-5)	6.46(-5)	1.25(-4)	1.9(-4)
Oxygen	4.1(-4)	7.41(-4)	4.17(-4)	3.1(-4)	5.5(-4)
Neon	1.0(-4)	1.20(-4)	1.23(-4)	1.0(-4)	1.1(-4)
Sodium	1.2(-6)	2.04(-6)		3.0(-6)	
Magnesium	2.2(-5)	3.8(-5)	2.4(-5)	2.5(-5)	2.1(-5)
Silicon	6.2(-6)	3.55(-5)	2.40(-5)	6.0(-6)	
Sulfur	9.4(-6)	1.86(-5)	1.23(-5)	7.1(-6)	7.9(-6)
Chlorine	1.1(-7)	1.86(-7)	1.86(-7)	2.0(-7)	
Argon	2.3(-6)	3.63(-6)		2.1(-6)	2.5(-6)
Potassium	4.9(-8)	1.35(-7)		1.48(-7)	
Calcium		2.19(-6)		3.8(-7)	
Iron		3.24(-5)	3.55(-5)		1.0(-6)

¹ Solar abundance from Grevesse & Noels (1993) and Anders & Grevesse (1989).

² O, B star abundances are the average of Gies & Lambert (1992) and Killian-Montenbruck et al. (1994).

ionization. These estimates were made using models, e.g. similarities on the ionization potential of some ions. Now, since the most important stages of ionization of several ions have been measured it can be checked how good the ionization correction factors, based on similarities in the ionization potential, are. There are two similarities introduced by Torres-Peimbert & Peimbert (1997). One is:

$$\frac{\text{Ne}}{\text{O}} = \frac{\text{Ne}^{++}}{\text{O}^{++}}. \quad (3)$$

Using the values given in Table 6 we find that $\text{Ne}/\text{O} = 0.16$ and $\text{Ne}^{++}/\text{O}^{++} = 0.15$. This is a very good agreement. Using the abundances for NGC 7027 given by Keyes & Aller (1990) a difference of 43% is found while using the abundances of Middlemass (1990) an agreement within 20% is found. The discussion becomes more problematic if, instead of using the 15.5 or 36.0 μm lines to compute the relative abundance of Ne^{++} , the optical line at 386.9 nm is used. This optical line gives a high Ne^{++} abundance, and the ratio for Ne/O and $\text{Ne}^{++}/\text{O}^{++}$ is 0.26 and 0.4 respectively, that is a difference of a 35%. It seems that depending on the lines used the ratio agrees or not.

The other similarity is:

$$\frac{\text{N}}{\text{O}} = \frac{\text{N}^+}{\text{O}^+}. \quad (4)$$

We find $\text{N}/\text{O} = 0.40$ and $\text{N}^+/\text{O}^+ = 0.59$, that is a difference of 32%. Other authors, i.e. Pottasch & Beintema (1999) found for this ratio in NGC 6302 a difference of 80%. This study indicates that ionization correction factors based on similarity in ionization potential are not well understood and should be used with caution.

Table 8. Comparison of the abundance ratios of C, N and O

	NGC 7027	Sun	O Stars
N/O	0.39	0.15	0.15
C/O	1.46	0.48	0.42
$\frac{\text{C+N+O}}{\text{H}}$	1.24(-3)	1.19(-3)	6.56(-4)

7.2. Physical parameters

N_e and T_e as a function of IP, that is, as a function of the distance to the central star have been obtained. The behavior of T_e as a function of IP is consistent with a simple picture of NGC 7027. This simple picture relates IP and distance to the central star: high ionization stages are reached close to the star and low stages occur in the outer parts. The O^{3+} 140.0 nm line gives a too high temperature. This line was taken from Keyes & Aller (1990) and they claim that it is blended with Si^{3+} . Decrease of this flux leads to a lower ratio, decreasing the temperature. In our opinion it is uncertain that the O^{3+} line is blended with the Si^{3+} line because it is a stellar line and should be formed close to the star. As the central star of NGC 7027 is very weak in the ultraviolet because of dust absorption, the Si^{3+} line will also be weak. The relation indicated in Fig. 3 is consistent with theory.

No trend of electron density with ions of low IP has been found, although it seems that there is a correlation of the density with ions at high ionization stages (high IP), where it seems to drop. This could mean that the ejection rate of the nebula in its latest stages was low because the highest ionization stages are reached close to the nebula and they give lowest density. This tells us that the mass

Table 9. Recombination and collisionally excited abundances

Ion	λ (nm)	Sort ¹	I_{obs}^2	$N_{\text{ion}}/N_{\text{p}}$
C ⁺⁺	190.9	Col	573	3.4(−4)
	426.7	Rec	0.559	5.2(−4)
N ⁺⁺	57 300	Col	1.296	9.1(−5)
	566.7	Rec	0.021	1.6(−4)
	567.9	Rec	0.022	9.8(−5)
O ⁺⁺	493.2	Col	0.230	1.8(−4)
	464.9	Rec	0.172	3.3(−4)
	407.2	Rec	0.104	4.3(−4)

¹ Col = Collisional excited line, Rec = Recombination line.

² Dereddened line intensities relative to $I_{\text{H}\beta} = 100$.

presently being ejected is considerably lower than at an earlier stage.

7.3. Abundances with recombination lines

A new problem has emerged in the study of nebular abundances. For some planetary nebulae it has been found that ionic abundances deduced from recombination lines are higher than those derived from collisionally excited lines. In a recent publication by Liu et al. (2000) a deep study in this sense is carried out for the planetary nebula NGC 6153. They have found that the abundance derived from optical recombination lines are a factor of 10 higher than those derived from optical, UV or infrared collisionally excited lines. This difference is significant. Liu et al. (2000) discuss density inhomogeneities and temperature fluctuations as the possible cause of such discrepancy, concluding that the latter are unimportant. Using the recombination lines measured by Keyes & Aller (1990) for NGC 7027 we have derived the abundances shown in Table 9.

These abundances have been derived by scaling those found by Liu et al. (2000). Although these lines give a somewhat higher abundance in the three cases compared, we do not regard this as significant and prefer to use the abundances found from the collisional lines. The great strength of the recombination lines in NGC 6153 remains a puzzle.

7.4. Abundances and progenitor

By comparing the abundances obtained with the semi-analytical model of Marigo et al. (1996), the mass of NGC 7027’s progenitor star can be constrained. With the derived abundances of helium, carbon, nitrogen and oxygen (Table 7) we can compare NGC 7027 to the model. The model predicts the chemical composition of planetary nebulae for two metallicities, $Z = 0.02$ and $Z = 0.008$. In the literature no clue to the metallicity of NGC 7027 is found. Then the central star has to be measured and this is not trivial. Because of this, the problem can be inverted. A clue in the metallicity of the central star can be given by

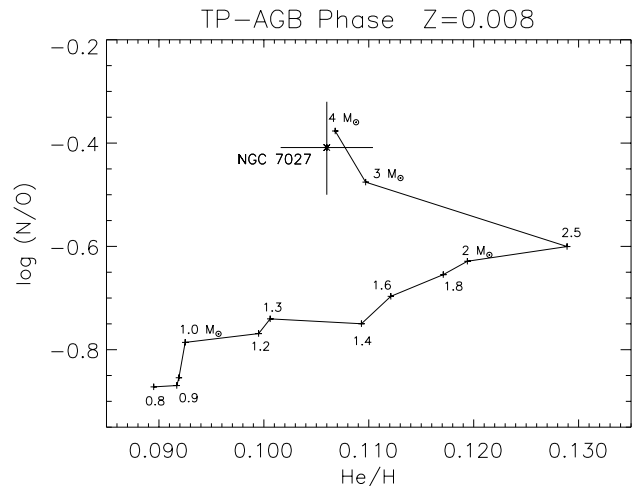


Fig. 4. The logarithm of N/O ratio versus He/H. Abundance ratios by number, expected in PN’s taken from the semi-analytical models of Marigo et al. 1996 (metallicity of $Z = 0.008$) are shown. The numbers in the figure indicate the mass of the progenitor star in solar units. The position of NGC 7027 is plotted

comparing the abundances derived with the different models of high or low metallicity and checking which one fits better. For this reason, the metallicity that better reproduces the NGC 7027 abundances was used ($Z = 0.008$).

As can be seen in Fig. 4 the model with a metallicity of $Z = 0.008$ constrains the mass of the star to be between 3–4 M_{\odot} . It is worth noticing that the model overestimates the prediction of the oxygen abundance with respect to the observational values. If the ratio C/O versus He/H or C/O versus N/O (where the overabundance of oxygen in the model is canceled) is considered, this leads to the conclusion that more carbon abundance is needed to fit the model. More studies concerning the carbon abundance and improvements in these evolutionary models are therefore needed.

8. Conclusions

A reliable infrared spectrum has been obtained (Table 2). This has been complemented with optical and ultraviolet lines in order to determine the physical parameters in the nebula, as well as to determine the abundances much more accurate than before. A correlation between electron temperature and IP has been found. Ions with high IP, that are formed close to the nebula, give high temperatures (around 15 000 K). Those with low IP, formed in the outer (coolest) parts give low temperature (see Fig. 3). No clear correlation of electron density with IP is found, although a tendency of density to decrease at high IP ion seems to be presented (Table 5 and Fig. 2). The relative and element abundances for 18 ions have been determined and are presented in Table 6. By comparing these abundances with the semi-analytical model of Marigo et al. (1996) at a metallicity $Z = 0.008$ we have constrained the mass of the progenitor star to be between 3–4 solar masses.

Acknowledgements. We are grateful to Peter van Hoof for his help with the atomic parameter data (especially the effective collision strength) used in our calculations

References

- Aller, L. H., & Hyung, S. 1995, *MNRAS*, 276, 1101
 Anders, E., & Grevesse, N. 1989, *Geochem. Cosmo.*, 53, 197
 Baars, J. W. M., Genzel, R., Pauliny-Toth, I. I. K., et al. 1977, *A&A*, 61, 99
 Benjamin, R. A., Skillman, E. D., & Smits, D. P. 1999, *ApJ*, 514, 307
 de Graauw, T., et al. 1996, *A&A*, 315, L49
 Fluks, M. A., Plez, B., Thé, P. S., et al. 1994, *A&AS*, 105, 311
 Gies, D. R., & Lambert, D. L. 1992, *ApJ*, 387, 673
 Grevesse, N., & Noels, A. 1993, in *Origin of the Elements*, ed. N. Prantos, et al. (Cambridge University Press), p. 15
 Hony, S., Van Kerckhoven, C., Peeters, E., et al. 2001, in preparation
 Hummer, D. G., & Storey, P. J. 1987, *MNRAS*, 224, 801
 Kaler, J. B., & Lutz, J. H. 1985, *PASP*, 97, 700
 Keenan, F. P., Aller, L. H., Bell, K. L., et al. 1999, *MNRAS*, 304, 27
 Keyes, C. D., & Aller, L. H. 1990, *PASP*, 102, 59
 Killian-Montenbruck, J., Grehen, T., & Nissen, P. E. 1994, *ApJ*, 291, 757
 Liu, X.-W., Barlow, M. J., Nguyen-Q-Rieu, et al. 1996, *A&A*, 315, L257
 Liu, X.-W., Storey, P. J., Barlow, M. J., et al. 2000, *MNRAS*, 312, 585
 Marigo, P., Bressan, A., & Chiosi, C. 1996, *A&A*, 313, 545
 Middlemass, D. 1990, *MNRAS*, 244, 294
 Peeters, E., Hony, S., Van Kerckhoven, C., et al. 2001, in preparation
 Persi, P., Cesarsky, D., Marenzi, A. R., et al. 1999, *A&A*, 351, 201
 Pottasch, S. R. 1984, *Planetary Nebulae*, D-Reidel, vol. 107
 Pottasch, S. R., & Beintema, D. A. 1999, *A&A*, 347, 975
 Roelfsema, P. R., Goss, W. M., Pottasch, S. R., & Zijlstra, A. 1991, *A&A*, 251, 611
 Shaw, R. A., & Kaler, J. B. 1982, *ApJ*, 261, 510
 Torres-Peimbert, S., & Peimbert, M. 1997, *IAU Symp.* 180, *Plan. Neb.*, ed. H. J. Habing, & H. J. G. L. M. Lamers, p. 175
 Van Kerckhoven, C., Hony, S., Peeters, E., et al. 2000, *A&A*, 357, 1013
 Walton, N. A., Pottasch, S. R., Reay, N. K., & Tailor, A. R. 1988, *A&A*, 200, L21
 Wolff, M. J., Code, A. D., & Groth, E. J. 2000, *AJ*, 119, 302